American Mineralogist, Volume 92, pages 1270–1275, 2007

Single-crystal X-ray diffraction study of high-pressure phases of $KHCO_3$

K. KOMATSU,[1,2,*] H. KAGI,[2] T. NAGAI,[3] T. KURIBAYASHI,[1] J.B. PARISE,[4] AND Y. KUDOH[1]

[1]Institute of Mineralogy, Petrology and Economic Geology, Graduate School of Science, Tohoku University, Sendai 980-8578, Japan
[2]Geochemical Laboratory, Graduate School of Science, The University of Tokyo, Tokyo 113-0033, Japan
[3]Division of Earth and Planetary Sciences, Graduate School of Science, Hokkaido University, Sapporo 060-0810, Japan
[4]Department of Geosciences and Chemistry, Mineral Physics Institute, Stony Brook University, Stony Brook, New York 11794-2100, U.S.A.

ABSTRACT

Monoclinic and triclinic high-pressure phases of $KHCO_3$ were identified using in situ high-pressure single-crystal X-ray analysis. These monoclinic and triclinic phases, designated as phases IV and V, respectively, differ from three previously identified phases: I–III. The lattices of the two phases are superimposed along $\mathbf{a}^*_{IV} = 2 \times \mathbf{a}^*_V$ and $hk0$ and $h0l$ nets of both phases lie on the same plane, i.e., the (100) plane is common in both lattices in real space. The space group of phase IV is $P2_1/b11$ with lattice constants of $a = 10.024(3)$ Å, $b = 6.912(5)$ Å, $c = 4.1868(11)$ Å, $\alpha = 115.92(4)°$, and $V = 260.9(2)$ Å^3. The crystal structure of phase IV, excluding the hydrogen atoms, was successfully determined by direct methods and is isostructural with a cesium hydrogen carbonate $CsHCO_3$.

Keywords: $KHCO_3$, high pressure, single-crystal X-ray diffraction, hydrogen bond

INTRODUCTION

When the donor moiety, *X*-H, forms a hydrogen bond (H bond) to an acceptor anion *Y*, i.e., *X*-H···*Y*, the potential energy curve becomes broader with shortening of the *X*···*Y* distance [*d*(*X*···*Y*)]. For strong hydrogen bonds [*d*(*X*···*Y*) is ca. 2.5 Å], an asymmetric double minimum develops (e.g., Fig. 1 in Novak 1974), and the barrier between the double minimum potential is reduced as *d*(*X*···*Y*) decreases. In strong hydrogen bonds, in some cases, the proton might transfer from donor to acceptor, i.e., *X*-H···*Y* → *X*···H-*Y*, a process facilitated by reducing the potential barrier. It is known that the ability of hydrogen bonds to transmit H^+ (or H_3O^+) and OH^- ions in water or an aqueous medium provides a catalysis mechanism for many reactions (e.g., Jeffrey 1997).

At extremely high-pressure conditions like in the deep Earth, almost all oxide minerals have close packing of oxygen with short *d*(O···O) to reduce their molar volume. The proton might be included in dense minerals, even those that are nominally anhydrous (Bell and Rossman 1992), resulting in the formation of strong H bonds. Although not often discussed in the Earth science context, proton transfer might play an important role in some physical properties and chemical reactions of minerals, including proton diffusion and hydrolysis in the deep Earth (e.g., Stillinger and Schweizer 1983).

Because of great interest in the dynamic nature of proton transfer, the H bond in potassium hydrogen carbonate $KHCO_3$ (kalicinite) has been studied using various techniques including X-ray and neutron diffraction methods. In an earlier work, Thomas et al. (1974a, 1974b) showed that the H bond associated with *d*(O···O) = 2.585(2) Å is moderately strong and that the protons occupy two possible sites in the H bond in the rough proportions of 4:1. In IR and Raman spectra of $KHCO_3$, the O-H stretching vibration exhibits a broad band between 1800 and 3500 cm^{-1} (Novak et al. 1963; Lucazeau and Noval 1973). A quasi-symmetric double minimum potential for the proton-stretching mode was proposed to explain the spectroscopic results (Fillaux 1983). A detailed inelastic neutron-scattering study (Ikeda et al. 2002) concluded that anharmonicity plays a major role and that proton dynamics cannot be represented using normal coordinates within the harmonic force-field approximation. Pressure is an attractive tool for understanding proton dynamics because, in principle, the *d*(O···O) associated with the H bond would decrease with decreasing volume, allowing the anharmonicity to be tuned continuously.

At atmospheric pressure, $KHCO_3$ undergoes an antiferrodistortive phase transition of an order-disorder type between phase I (Fig. 1a; high-temperature phase, space group: $C2/m$) and phase II (Fig. 1b; low-temperature phase, space group: $P2_1/a$) at T_N = 318 K (Kashida and Yamamoto 1990). Two (HCO_3^-) groups in the crystal are bonded by two H bonds and form $(HCO_3^-)_2$ dimers. These dimers have two stable rotational angles around the **c** axis, which were drawn as right and left-inclined bold lines in Figure 1. These dimers are disordered in phase I and ordered with an anti-phase configuration in phase II.

Recently, new polymorphs of $KHCO_3$ have been reported by several investigators (Takasaka et al. 2002; Nagai et al. 2002; Kagi et al. 2003, 2005). One of the polymorphs is phase III, which is promoted by shear stress (Takasaka et al. 2002). Although the crystal structure of phase III has not been determined, Kerst et al. (1995) reported the appearance of triclinic ferroelastic domains [space group $C1$ or C, $a = 15.182(3)$ Å, $b = 5.6320(3)$ Å, $c =$

* Present address: Centre for Science at Extreme Conditions, The University of Edinburgh, Edinburgh EH9 3JZ, U.K. E-mail: kom@eqchem.s.u-tokyo.ac.jp

0003-004X/07/0809–1270$05.00/DOI: 10.2138/am.2007.2392

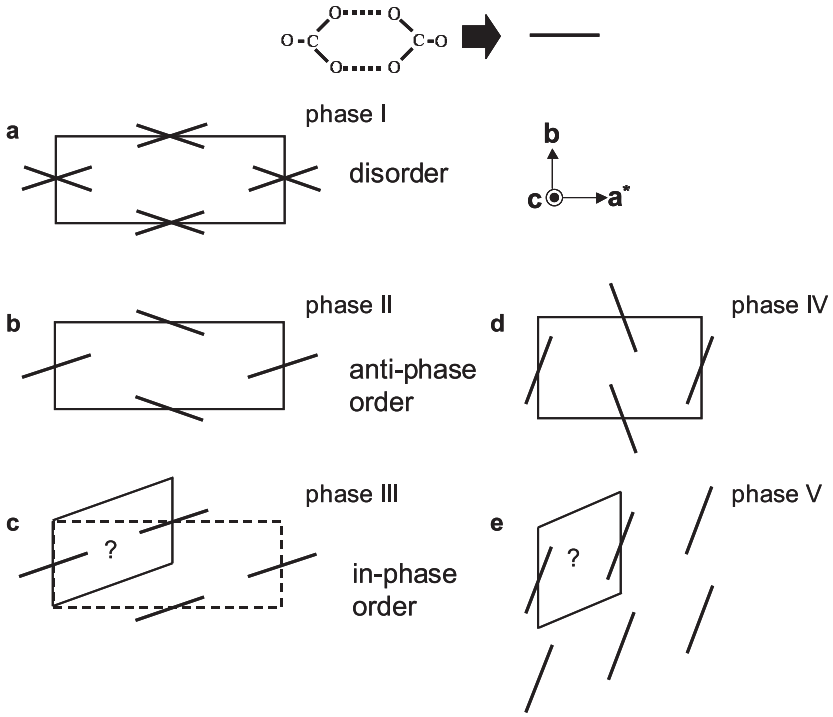

FIGURE 1. Configuration of $(HCO_3)_2$ dimers on a *c*-plane projection (modified after Fig. 1 in Takasaka et al. 2002). Each dimer is represented by a thick solid line. Each unit cell is designated by solid parallelograms. (**a**) Phase I with disordered configuration of dimers. (**b**) Phase II with anti-phase configuration of dimers. (**c**) Phase III with in-phase configuration of dimers. The dotted rectangle denotes the unit cell described by the non-standard triclinic setting (*C*1 or $C\bar{1}$; Kerst 1995), which can be compared to the unit cell of phases I and II. (**d**) Phase IV with anti-phase configuration of dimers. (**e**) Phase V with in-phase configuration of dimers. The crystal structures of phases III and V have not been confirmed by diffraction methods. Therefore, those configurations remain open to question.

3.7131(1) Å, $\alpha = 89.554(4)°$, $\beta = 104.640(3)°$, $\gamma = 92.101(4)°$] when uniaxial pressure is applied to $KHCO_3$ below T_N. Le Grand et al. (1998) reported ferroelastic domains coexisting with the monoclinic phase in as-grown $KHCO_3$ crystals below T_N. Takasaka et al. (2002) observed Brillouin scattering under shear stress and discovered a ferrodistortive phase having in-phase configuration of dimers and they designated it as phase III (Fig. 1c; Takasaka et al. 2002). Takasaka et al. (2002) also concluded that the ferroelastic phase reported by the previous authors (Kerst 1995; Le Grand et al. 1998) corresponds to phase III, which is a ferrodistortive and is also a ferroelastic phase with space group *P* (*C* in a non-standard setting). Another polymorph is an unassigned phase discovered at high-pressure by powder X-ray diffraction study (Nagai et al. 2002). This high-pressure phase results from a reversible phase transition observed at 2.8 GPa, a transition pressure subsequently confirmed by powder neutron diffraction, IR and Raman spectroscopic studies (Kagi et al. 2003). Kagi et al. (2005) compared the pressure response of the crystal structure, especially surrounding the H bond, between $KHCO_3$ and $NaHCO_3$. Although some experimental results have been reported, the crystal structure of the high-pressure phase and the mechanism of the pressure-induced phase transition remain unclear. In this study, the crystal structure of the high-pressure phase of $KHCO_3$ was determined by analysis of single-crystal synchrotron X-ray diffraction data collected from a sample mounted in diamond anvil cells (DACs).

EXPERIMENTAL METHODS

Prismatic single crystals 50–200 μm on edge of phase II were grown from K_2CO_3 aqueous solution using slow evaporation at room temperature. A modified Merrill-Bassett type DAC (Kudoh and Takeda 1986) was used for the high-pressure experiment. A 250 μm thick SUS301 stainless steel plate with a 300 μm diameter hole in the center was used as a gasket. A 4:1 methanol-ethanol mixture was used for the pressure-transmitting medium. To avoid the extra diffraction signal, no ruby chip was mounted for determining pressure. Pressure was increased stepwise and a phase transition, accompanied by abrupt change in sample shape, was observed visually (Fig. 2). Interestingly, two domains were optically observed just after the phase transition (Fig. 2a), and the number of domains increased with time (Fig. 2b). Above the phase transition pressure, X-ray oscillation photographs were taken using an imaging plate X-ray diffractometer (R-AXIS IV^{++}; Rigaku Corp.) with a rotating anode (Mo*K*α, 50 kV, 80 mA). The observed reflections were indexed as a mixture of a monoclinic and a triclinic phase, as described later.

Pressure was determined approximately from the Raman band of the methanol-ethanol mixture in the DAC, instead of the usual ruby fluorescence method. Raman spectra were measured using a spectrometer (NRS-2000; Jasco Inc.) with a nitrogen-cooled CCD detector. A microscope was used to focus the excitation laser beam (514.5 nm line Ar^+ laser; Princeton Instruments Inc.). The ν_{CC} stretching mode of a methanol-ethanol mixture was observed at 899 cm^{-1}. Wang et al. (2004) showed that the ν_{CC} stretching mode was observed at 882 cm^{-1} at ambient conditions, and that the frequency of this mode increased linearly by 3.7 cm^{-1}/GPa with increasing pressure. Hence, the pressure was estimated at about 4.6 GPa. Although we were not able to evaluate strictly the estimated standard deviation of this pressure value due to the lack of information about the error of the pressure dependence of the ν_{CC} stretching mode in the previous study, it is expected that the estimated pressure has relatively large uncertainty of ca. 0.5 GPa (see Fig. 3 in Wang et al. 2004). All X-ray diffraction measurements in this study were carried out at this pressure.

X-ray diffraction measurements for determining the unit-cell parameters and for collecting intensities of the monoclinic phase were performed using a four-circle X-ray diffractometer installed at the beam line BL-10A, Photon Factory, KEK, Tsukuba, Japan. The wavelength of the synchrotron radiation was calibrated as $\lambda = 0.6990(2)$ Å from the unit-cell constants of a ruby standard crystal at ambient conditions. The cell parameters were determined by 27 centered reflections in the 2θ range of 35–45°. The X-ray diffraction intensities were collected up to $\sin\theta/\lambda < 0.82$ Å^{-1} (maximum 2θ is 70°) by the ω-scan with the fixed φ method (Finger and King 1978). Absorption corrections for the Be backing plates and a pair of diamonds of the DAC were carried out according to the method described by Angel (2004). Extinction and absorption corrections of the crystal were not applied. The observed intensities were corrected for Lorentz and polarization effects.

The crystal structure excluding hydrogen atoms was solved by direct methods

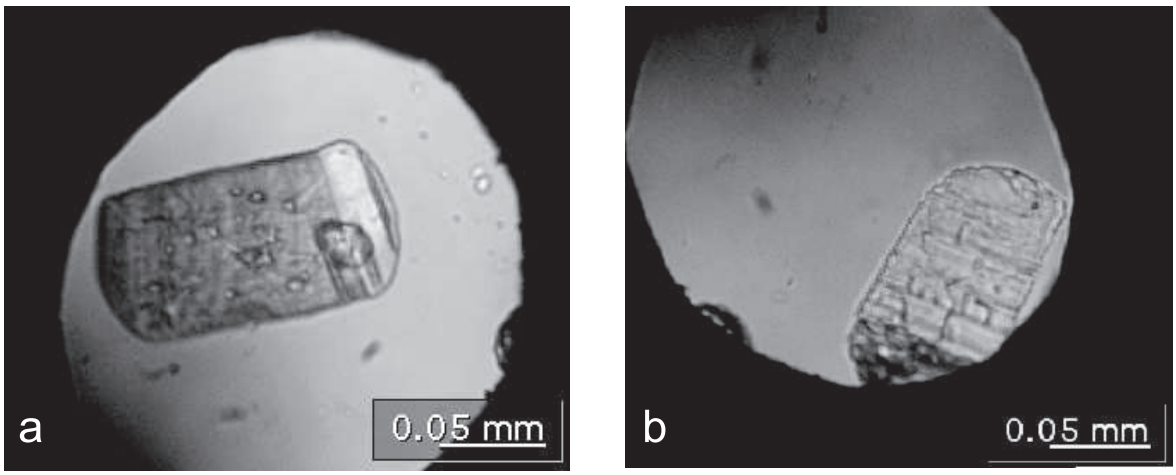

FIGURE 2. Visually observed phase transition of $KHCO_3$ in DAC under the polarized microscope. (**a**) Immediately after transition and (**b**) after 24 h.

using the Sir2004 program package (Burla et al. 2005). Fractional atomic coordinates and isotropic atomic displacement parameters for non-hydrogen atoms were refined using SHELXL of the SHELX-97 program package (Sheldrick 1997). The final cycle of full-matrix least-squares refinement on F^2 was based on 439 observed reflections [$F_o > 4.00\sigma F_o$] and 22 variable parameters. No geometrical constraints or restraints were applied in the refinement.

RESULTS AND DISCUSSION

Assignment of reciprocal lattices

Bragg reflections in the observed X-ray oscillation photographs above the phase transition pressure were assigned to a monoclinic and triclinic lattice. (Fig. 3). These lattices were different from the three polymorphs described previously (phases I–III; Fig. 1). Although both settings of these monoclinic and triclinic lattices are non-standard, these settings were chosen to facilitate comparison with the ambient pressure phase (phase II), as described later. Hereafter, the monoclinic phase is designated as phase IV and the triclinic phase as phase V. Figure 3 shows that the two lattices are superimposed on the **a*** axis with $\mathbf{a}_{IV}^* = 2 \times \mathbf{a}_V^*$ and *hk*0 and *h*0*l* nets of both phases lie on the same plane: the (100) plane is common to both lattices in real space. Overlapped reflections, *h*00, were included in the Fourier synthesis with a separate scale factor in addition to the overall scale factor. Diffuse streaks parallel to the **a*** axis, indicative of lamellar stacking disorder of the common (100) planes of phases IV and V, were observed frequently (Fig. 4).

The unit-cell parameters were determined from data collected on a four-circle X-ray diffractometer at the BL-10A beamline. Crystal data and structural refinement parameters for phase IV are listed in Table 1. The unit-cell parameters of phase V have not been refined precisely. The approximate values calculated from the observed Bragg reflections in oscillation photographs are $a_V \approx 5.44$ Å, $b_V \approx 6.91$ Å, $c_V \approx 4.2$ Å, $\alpha_V \approx 115°$, $\beta_V \approx 94°$, and $\gamma_V \approx 69°$. The space group of phase IV [$P2_1/b11$ (no. 14)] is determined uniquely from reflection conditions (0*kl*: $k = 2n$ and *h*00: $h = 2n$). This non-standard setting ($P2_1/b11$; **a**, **b**, **c**) can be transformed to the standard monoclinic setting ($P12_1/c1$; **a'**, **b'**, **c'**) through the following transformation matrix:

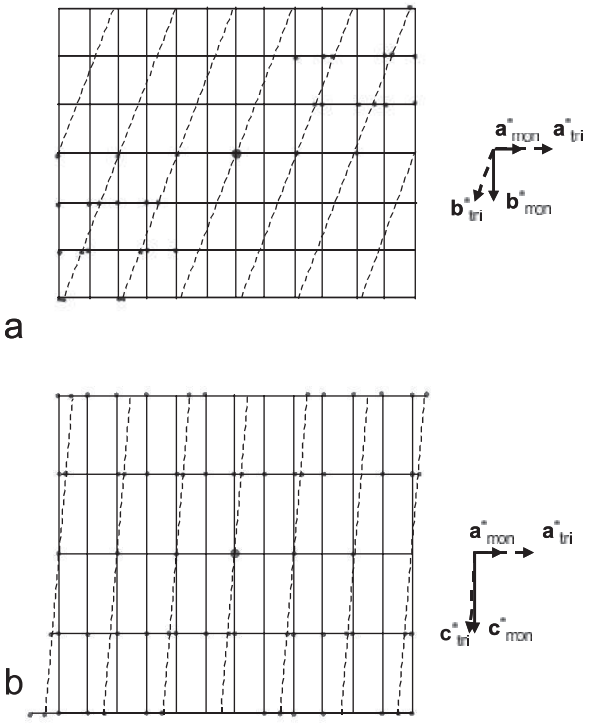

FIGURE 3. Schematic drawings of observed reflections on (**a**) the *hk*0 net and (**b**) the *h*0*l* net. Observed reflections were assigned to a monoclinic lattice with $a_{IV}^* \approx 0.10$ Å^{-1}, $b_{IV}^* \approx 0.16$ Å^{-1}, $c_{IV}^* \approx 0.26$ Å^{-1}, and $\alpha_{IV}^* \approx 64°$ and a triclinic lattice with $a_V^* \approx 0.20$ Å^{-1}, $b_V^* \approx 0.17$ Å^{-1}, $c_V^* \approx 0.27$ Å^{-1}, $\alpha_V^* \approx 64°$, $\beta_V^* \approx 96°$, and $\gamma_V^* \approx 111°$. The observed triclinic axes of phase V are related to the axes of phase IV as $\mathbf{a}_V \approx 0.503\ \mathbf{a}_{IV} + 0.318\ \mathbf{b}_{IV} + 0.131\ \mathbf{c}_{IV}$, $\mathbf{b}_V = \mathbf{b}_{IV}$, and $\mathbf{c}_V = \mathbf{c}_{IV}$. The solid circles represent the observed reflection calculated from the positions in the imaging plate. The solid lines and the broken lines respectively represent the monoclinic component and the triclinic component. A few reflections were observed in the *hk*0 net because most reflections in the *hk*0 net were in the blind region by the DAC.

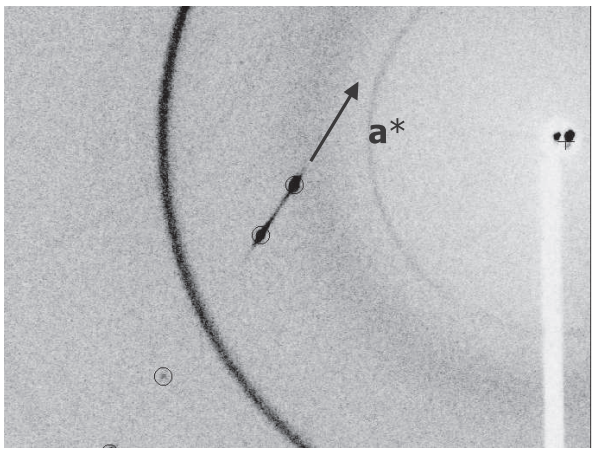

FIGURE 4. A representative X-ray oscillation photograph showing diffuse streaks on the diffraction spots parallel to **a***. The positions of diffraction spots are indicated by circles.

$$\begin{pmatrix}\mathbf{a'} & \mathbf{b'} & \mathbf{c'}\end{pmatrix} = \begin{pmatrix}\mathbf{a} & \mathbf{b} & \mathbf{c}\end{pmatrix}\begin{pmatrix}0 & -1 & 0\\ -1 & 0 & 1\\ -1 & 0 & 0\end{pmatrix}$$

The setting for phase V has **b** and **c** axes in common with phase IV.

Crystal structure and H bond of high-pressure phases

Following solution of the crystal structure of phase IV, excluding hydrogen atoms, the isostructural relationship to the structure of $CsHCO_3$ at ambient conditions was revealed. The fractional atomic coordinates and isotropic atomic displacement parameters for non-hydrogen atoms are shown in Table 2. For comparison to the ambient pressure phase, the crystal structures of phase II and IV are drawn in Figures 5a and 5b, respectively. In phase II, the dimers consisting of two CO_3 group lie approximately on the plane parallel to $(\bar{3}01)$, and ones in phase IV lie on the plane parallel to (011). These sets of two CO_3 groups are shown as ellipses in Figure 5. In phase II, two CO_3 groups assume one of the two orientations, which are symmetric with respect to the **a*** axis and ordered in an anti-phase configuration (Fig. 5a; see also Fig. 1b). Two orientations, which are also symmetric to the **a*** axis, exist in phase IV and the two CO_3 groups are ordered in an anti-phase configuration (Fig. 5b; see also Fig. 1d). The non-standard setting of phase IV adopted in this study clarifies the relationship between crystal structures of the ambient pressure phase II and high-pressure phase IV.

In ambient pressure phases I, II, and probably also in phase III, two CO_3 molecules in the crystal are bonded by two H bonds to form $(HCO_3^-)_2$ dimers. A Fourier difference map was calculated using data with $\sin\theta/\lambda < 0.489$ (maximum 2θ is 40°) to maximize contributions from possible hydrogen positions. It is generally difficult to find hydrogen sites with sufficient accuracy based on X-ray diffraction data, especially under high-pressure conditions, due to both the low atomic scattering of hydrogen and the uncertainties in observed intensities resulting from parasitic elastic and inelastic scattering from DACs. In this case, however, a residual peak between O2 and O3 sites was observed in the Fourier difference map (Fig. 6). The d(O2···O3) was 2.502(11) Å, a value significantly less than that observed in phase II of 2.585(2) Å (Thomas et al. 1974a). The relatively low residual peak, which has a height of 0.5 eÅ^{-3},might result from a mobile hydrogen atom disordered between donor and acceptor oxygen atoms in such a strong hydrogen bond.

The H-bond distance, d(O2···O3), is also quite consistent with previous spectroscopic data. Kagi et al. (2003) obtained the IR spectra of $KHCO_3$ at pressures up to 6.3 GPa. According to their results, a broad band centered at approximately 2600 cm^{-1} is attributable to the O-H stretching mode. No significant change in the frequency of the O-H stretching frequency can be found with increasing pressure. In such strong H-bond compounds, for the value of the d(O···O) ≈ 2.6Å, it is predicted that Fermi resonance exists between the fundamental of the O-H stretching mode [ν_{OH}(0-1)] and the overtones of the bending modes [σ_{OH}(0-2) and γ_{OH}(0-2)]. Ikeda et al. (1998) presented a simple numerical model for the H bond and the values calculated for ν_{OH} along with d(O···O) were consistent with the observed values. According to Ikeda et al. (1998) the value of ν_{OH} of 2600 cm^{-1} corresponds to d(O···O) ≈ 2.5–2.6 Å, which is as long as the observed d(O2···O3) of 2.502(11) Å in phase IV. Moreover, in

TABLE 1. Crystal data and structural refinement parameters for high-pressure monoclinic phase (phase IV) of $KHCO_3$

Pressure (GPa*)	4.6
Molecular weight	400.39
F_{000}	200.0
Space group	$P2_1/b11$†
Diffractometer	Four-circle diffractometer (BL-10A, PF, KEK)
Unit-cell parameters	
a (Å)	10.024(3)
b (Å)	6.912(5)
c (Å)	4.1868(11)
α (°)	115.92(4)
Unit-cell volume, V_c (Å^3)	260.9(2)
Z	4
Density (calculated) d (g·cm^{-3})	2.55
X-ray source	Synchrotron radiation
Wavelength λ (Å)	0.6990(2)
Index ranges	$-15 \le h \le 4$ $-7 \le k \le 6$ $-6 \le l \le 6$
No. observations [$F_o > 4.00\sigma F_o$]	439
No. variables	22
Reflection/Parameter ratio	19.95
R_1‡ [$F_o > 4.00\sigma F_o$]	0.0858
wR_2§	0.2343
Goodness-of-fit‖	1.032

* Pressure was estimated approximately by the wavenumber of Raman spectra of the 4:1 methanol-ethanol mixture.
† The standard setting for the monoclinic structure is $P12_1/c1$ (no. 14) with a = 6.321(5) Å, b = 10.024(3) Å, c = 6.912(5) Å, β = 143.45(3)°. The above setting ($P2_1/b11$) is used to facilitate comparison with the ambient pressure phase (phase II).
‡ $R_1 = \Sigma||F_o| - F_c||/\Sigma|F_o|$.
§ $wR_2 = \{\Sigma[w(F_o^2 - F_c^2)^2]/\Sigma[w(F_o^2)^2]\}^{1/2}$, $w = 1/[\sigma^2(F_o^2) + (aP)^2 + bP]$, where $P = (F_o^2 + 2F_c^2)/3$ and a and b are adjustable parameters.
‖ Goodness-of-fit = $S = \{\Sigma[w(F_o^2 - F_c^2)^2]/(n-p)\}^{1/2}$, where n is the number of reflections and p is the total number of refined parameters.

TABLE 2. Refined fractional atomic coordinates and isotropic displacement parameters for phase IV of $KHCO_3$

Atom	x/a	y/b	z/c	U_{iso} (Å^2)
K	0.32167(17)	0.5869(4)	0.4345(4)	0.0168(5)
C	0.0456(7)	0.705(2)	0.8191(19)	0.017(2)
O1	0.0806(5)	0.8352(15)	0.6998(13)	0.0218(13)
O2	0.9244(5)	0.6632(15)	0.8584(14)	0.0210(12)
O3	0.1397(5)	0.6120(13)	0.9320(11)	0.0191(12)

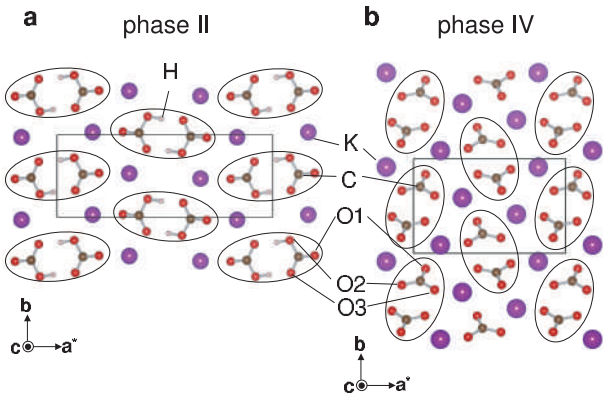

FIGURE 5. The crystal structures of (**a**) the ambient pressure phase (phase II) and (**b**) the high-pressure monoclinic phase (phase IV). Only H1 site in phase II and no hydrogen sites in phase IV are described. The $(HCO_3^-)_2$ dimers are included in the ellipses. Each unit cell is designated by parallelograms.

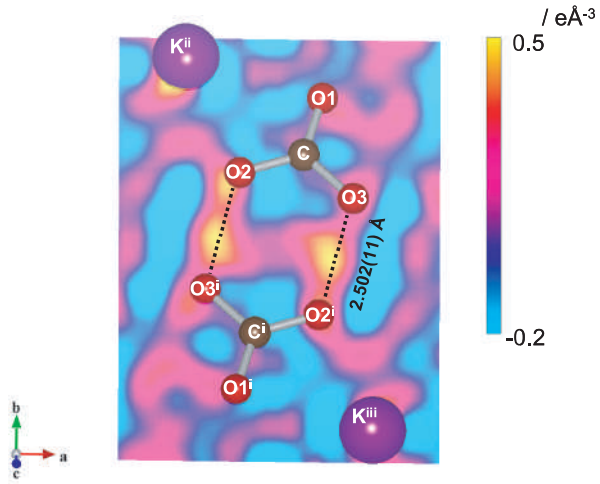

FIGURE 6. A Fourier difference map section with a ball-and-stick model of phase IV. This section is parallel to the (011) plane, and the two CO_3 groups approximately lie in the section. Symmetry codes are (i) $-x$, $1-y$, $2-z$; (ii) $-1/2+x$, $3/2-y$, $1-z$; (iii) $1/2-x$, $-1/2+y$, $1+z$.

$CsHCO_3$, which has the same non-hydrogen structure as phase IV of $KHCO_3$ (Kaduk 1993), the hydrogen site also corresponds with the site shown in the Fourier difference map of phase IV. Accordingly, it is concluded that two CO_3 molecules in phase IV are bonded by two H bonds to form $(HCO_3^-)_2$ dimers as in the ambient pressure phases.

"Broken symmetry" of orientations of two CO_3 groups and the mechanism of phase transition

The observation that the two lattices of phases IV and V are superimposed along the **a*** axis and that $\mathbf{a}_{IV}^* = 2 \times \mathbf{a}_V^*$ strongly suggests that phase V might be ordered with an in-phase configuration of two CO_3 groups, as illustrated in Figure 1e. It is likely that phase V contacts with phase IV along the (100) plane; also, the d_{100} of phase IV is two times larger than that of phase V, which might be explained by the configuration of two CO_3 groups as shown in Figures 7a and 7b. Accordingly, the observed

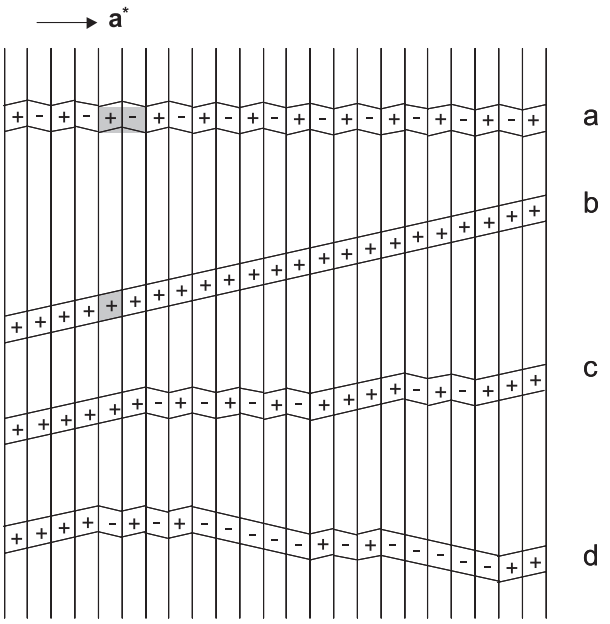

FIGURE 7. Schematic drawings of the relationship between the structures of (**a**) phase IV and (**b**) phase V in terms of the orientations of dimers parallel to (100) planes. Each unit cell is shaded. Two possible orientations of dimers are labeled + and –. Only one of the two possible orientations was described as a phase V structure in **b**. (**c**) The observed relationship between phases IV and V. (**d**) The possible but unobserved relationship between phases IV and V.

relationship of phase IV and V can be drawn schematically as in Figure 7c. Note that a possible (100) twin for phase V was not seen in this experiment. If two CO_3 groups in phase V randomly adopt one of the two orientations, which are symmetric with respect to the **a*** axis and the ordered structure in the in-phase configuration, both orientations should be statistically adopted in a crystal as shown in Figure 7d. This "broken symmetry" of orientations of two CO_3 groups could be key information allowing elucidation of the mechanism of the phase transition as discussed later.

The phase transition between phase II and phase IV is obviously first-order, because the unit-cell volume of phase IV of 260.9(2) Å^3 at 4.6 GPa is significantly less than the extrapolated value of 267.8(4) Å^3 of phase II [V_0 = 311.1(1) Å^3, K_0 = 22.7 (3) GPa, and K' = 4 (fixed); see also Fig. 2 in Nagai et al. 2002]. Moreover, the observation that the phase transition is accompanied by an instantaneous change of the crystal shape also supports the conclusion that this structural phase transition is first-order.

Why does a single phase (phase II) transform to two different phases (phase IV and V) at the same pressure? It is unlikely, though not impossible, that the triple point at which phases II, IV, and V can coexist is coincidentally at 2.8 GPa and room temperature. One possible explanation for the coexistence of phases IV and V is that shear stress causes an intergrowth of these two phases. If the crystal structure of phase V has an ordered structure with an in-phase configuration of two CO_3 groups similar to phase III, a similar phase transition by shear stress in the case of phase III could be possible. In addition, the transition by shear stress

may be able to explain the "broken symmetry" of orientations of two CO_3 groups. However, a question remains whether such shear stress significantly exists in the DACs using methanol-ethanol mixture as a pressure-transmitting medium. Another possible explanation for the coexistence of the two phases is that phase V corresponds to a high-pressure form of phase III. Le Grand et al. (1998) described observations of coexistence of thin ferroelastic domains (phase III) in as-grown $KHCO_3$ crystals (phase II) below T_N under the polarizing microscope. Interestingly, Le Grand et al. (1998) indicated that an X-ray investigation of this thin domain of phase III is not possible due to the small diffractive volume. Thus, it is possible that the thin domain of phase III in phase II underwent the phase transition under pressure and nucleated the coexisting phase V in phase IV. In this interpretation, however, the observed "broken symmetry" seems to remain an open question. The crystal structure of phases III and V, which may have the in-phase configurations of dimers, and the physical mechanism of the phase transition requires further investigation.

Acknowledgments

The authors are most grateful to Przemyslaw Dera, who first pointed out that the crystal structure of phase IV of $KHCO_3$ is isostructural with $CsHCO_3$ and made a lot of helpful comments. Figures 5 and 6 were drawn with VESTA developed by Momma and Izumi (2006). This work was supported by the Ministry of Education, Culture, Sports, Science, and Technology (MEXT) of Japan, via a Grant-in-Aid for JSPS Fellows, 4681, 2005. This work was also supported by a Grant-in-Aid for The 21st Century COE Program for Advanced Science and Technology Center for the Dynamic Earth, and the Frontiers in Fundamental Chemistry of MEXT. J.B.P. is grateful for the support of NSF grants EAR-0510501 and DMR-0452444.

References cited

Angel, R.J. (2004) Absorption corrections for diamond-anvil pressure cells implemented in the software package Absorb 6.0. Journal of Applied Crystallography, 37, 486–492.

Bell, D.R. and Rossman, G.R. (1992) Water in earth's mantle: The role of nominally anhydrous minerals. Science, 255, 1391–1397.

Burla, M.C., Caliandro, R., Camalli, M., Carrozzini, B., Cascarano, G.L., De Cano, L., Giacovazzo, C., Polidori, G., and Spagna, R. (2005) Sir2004: An improved tool for crystal structure determination and refinement. Journal of Applied Crystallography, 38, 381–388.

Fillaux, F. (1983) Calculations of infrared and Raman band profiles of strong hydrogen bonds, OH stretching bands and proton dynamics in crystalline potassium hydrogen carbonate. Chemical Physics, 74, 405–412.

Finger, L.W. and King, H. (1978) A revised method of operation of the single-crystal diamond cell and refinement of the structure of NaCl at 32 kbar. American Mineralogist, 63, 337–342.

Ikeda, S., Sugimoto, H., and Yamada, Y. (1998) Isotope effects and Fermi resonance in hydrogen bonds: A new model. Physical Review Letters, 81, 5449–5452.

Ikeda, S., Kashida, S., Sugimoto, H., Yamada, Y., Bennington, S.M., and Fillaux, F. (2002) Inelastic neutron scattering study of the localized dynamics of protons in $KHCO_3$ single crystals. Physical Review B, 66, 184302.

Jeffrey, G.A. (1997) An introduction to hydrogen bonding, p. 119–123. Oxford University Press, New York.

Kaduk, J.A. (1993) Crystal structure of caesium hydrogen carbonate. Zeitschrift für Kristallographie, 205, 319–320.

Kagi, H., Nagai, T., Loveday, J.S., Wada, C., and Parise, J.B. (2003) Pressure-induced phase transformation of kalicinite ($KHCO_3$) at 2.8 GPa and local structural changes around hydrogen atoms. American Mineralogist, 88, 1446–1451.

Kagi, H., Nagai, T., Komatsu, K., Okada, T., Wada, C., Loveday, J.S., and Parise, J.B. (2005) Pressure response on hydrogen bonds in potassium hydrogen carbonate and sodium hydrogen carbonate. Journal of Neutron Research, 13, 21–26.

Kashida, S. and Yamamoto, K. (1990) Structural phase transition in $KHCO_3$. Journal of Solid State Chemistry, 86, 180–187

Kerst, H. (1995) Phasenumwandlungen bei $KHCO_3$ und $KDCO_3$. Ph.D. thesis, Institute für Kristallographie, RWTH Aachen, Germany.

Kudoh, Y. and Takeda, H. (1986) Single crystal X-ray diffraction study on the bond compressibility of fayalite, Fe_2SiO_4 and rutile, TiO_2 under high-pressure. Physica B, 139–140, 333–336.

Le Grand, Y., Rouède, D., Wienold, J., and Glinnemann, J. (1998) Light refraction at the interface between coexisting phases of $KHCO_3$. Journal of the Physical Society of Japan, 67, 1451–1456.

Lucazeau, G. and Noval, A. (1973) Low temperature Raman spectra of $KHCO_3$ single crystal. Journal of Raman Spectroscopy, 1, 573–586.

Momma, K. and Izumi, F. (2006) An integrated three-dimensional visualization system, VESTA, using wxWidgets. Commission on Powder Diffraction, IUCr Newsletter, 7, 106–119.

Nagai, T., Kagi, H., and Yamanaka, T. (2002) The first observation of a pressure-induced phase transition and compression behavior of kalicinite ($KHCO_3$) at room temperature. Solid State Communication, 123, 371–374

Novak, A. (1974) Hydrogen bonding in solids: Correlation of spectroscopic and crystallographic data. Structure and Bonding, 18, 177–216.

Novak, A., Saumagne, P., and Bok, L.D.C. (1963) An infrared spectroscopic study of some alkali bicarbonates: $NaHCO_3$, NH_4HCO_3, $KHCO_3$, and sodium sesquicarbonate $Na_2CO_3{\cdot}NaHCO_3{\cdot}2H_2O$. Journal de Chimie Physique, 60, 1385–1395.

Sheldrick, G.M. (1997) SHELXL97. Program for the refinement of crystal structure. University of Göttingen, Germany.

Stillinger, F.H. and Schweizer, K.S. (1983) Ice under pressure: transition to symmetrical hydrogen bonds. Journal of Physical Chemistry, 87, 4281–4288.

Takasaka, S., Tsujimi, Y., and Yagi, T. (2002) Shear-stress-induced phase transition in $KHCO_3$ studied by Brillouin scattering. Physical Review B, 65, 174102.

Thomas, J.O., Tellgren, R., and Olovsson, I. (1974a) Hydrogen-bond studies. LXXXIV. An X-ray diffraction study of the structures of $KHCO_3$ and $KDCO_3$ at 298, 219 and 95 K. Acta Crystallographica B, 30, 1155–1166.

——— (1974b) Hydrogen-bond studies. XCII. Disorder in $(HCO_3)_2^{2-}$ and $(DCO_3)_2^{2-}$ dimers: A neutron diffraction study of $KHCO_3$ and $KDCO_3$. Acta Crystallographica B, 30, 2540–2548.

Wang, X.B., Shen, Z.X., Tang, S.H., and Kuok, M.H. (2004) Near infrared excited micro-Raman spectra of 4:1 methanol-ethanol mixture and ruby fluorescence at high pressure. Journal of Applied Physics, 18, 8011–8017.

Manuscript received July 19, 2006
Manuscript accepted March 30, 2007
Manuscript handled by Przemyslaw Dera